

An updated catalog of OH-maser-emitting planetary nebulae

L. Uscanga^{1,2}, J.F. Gómez², O. Suárez³, and L.F. Miranda^{4,5}*

¹ Observatorio Astronómico Nacional (IGN), Alfonso XII No. 3, E-28014 Madrid, Spain email: l.uscanga@oan.es

² Instituto de Astrofísica de Andalucía, CSIC, Apartado 3004, E-18080 Granada, Spain

³ Laboratoire Lagrange, UMR7293, Université de Nice Sophia-Antipolis, CNRS, Observatoire de la Côte d'Azur, 06304 Nice Cedex 4, France

⁴ Consejo Superior de Investigaciones Científicas, C/ Serrano 117, E-28006, Madrid, Spain

⁵ Departamento de Física Aplicada, Facultade de Ciencias, Universidade de Vigo, E-36310 Vigo, Spain

Preprint online version: September 27, 2012

ABSTRACT

Aims. We studied the characteristics of planetary nebulae (PNe) that show both OH maser and radio continuum emission (hereafter OHPNe). These have been proposed to be very young PNe, and therefore, they could be key objects for understanding the formation and evolution of PNe.

Methods. We consulted the literature searching for interferometric observations of radio continuum and OH masers toward evolved stars, including the information from several surveys. We also processed radio continuum and OH maser observations toward PNe in the Very Large Array data archive. The high positional accuracy provided by interferometric observations allow us to confirm or reject the association between OH maser and radio continuum emission.

Results. We found a total of six PNe that present both OH maser and radio continuum emissions, as confirmed with radio interferometric observations. These are bona fide OHPNe. The confirmed OHPNe present a bipolar morphology in resolved images of their ionized emission at different wavelengths, suggesting that the OH maser emission in PNe is related to nonspherical mass-loss phenomena. The OH maser spectra in PNe present a clear asymmetry, tending to show blueshifted emission with respect to the systemic velocity. Their infrared colors suggest that most of these objects are very young PNe. OHPNe do not form a homogeneous group, and seem to represent a variety of different evolutionary stages. We suggest that OH masers pumped in the AGB phase may disappear during the post-AGB phase, but reappear once the source becomes a PN and its radio continuum emission is amplified by the OH molecules. Therefore, OH maser emission could last significantly longer than the previously assumed 1000 yr after the end of the AGB phase. This maser lifetime may be longer in PNe with more massive central stars, which ionize a larger amount of gas in the envelope.

Key words. masers – stars: AGB and post-AGB – ISM: planetary nebulae: general

1. Introduction

Planetary nebulae (PNe) are a phase in the evolution of low and intermediate mass stars ($\leq 8M_{\odot}$), after they have passed through both the asymptotic giant branch (AGB) phase and a brief, 10^2 to 10^4 yr, post-AGB phase (Blöcker 1995). The effective temperature of the central star increases rapidly during this last phase, until at $\sim 30,000$ K its radiation begins to ionize the circumstellar shell, whereupon it becomes a PN (Kwok 1993). The ionized gas of PNe is detected at radio wavelengths from its free-free radiation. Radio continuum observations thus provide an important diagnostic for PNe per se, as well as information about their physical structure and properties (e.g., electron density, mass).

The circumstellar envelopes of oxygen-rich evolved stars provide optimal conditions for pumping masers of different species. Maser emission of SiO, H₂O, and OH is detected from AGB envelopes, and it tends to be stratified, with SiO masers located close to the central star (~ 10 AU), H₂O masers located in the inner part of the envelope (between 10 and 100 AU) and OH masers at distances $> 10^3$ AU from the central star (Reid & Moran 1981). In the particular case of OH maser emission, the spectra usually show the double-peaked profiles charac-

teristic of spherical envelopes expanding at velocities of ~ 10 – 30 km s⁻¹ (Reid et al. 1977; Bowers et al. 1989).

OH masers are expected to disappear ≈ 1000 yr after the AGB mass-loss stops (Lewis 1989; Gómez et al. 1990). Consequently, in some early PNe, the inner part of the envelope could already be ionized, while the outer regions are still neutral. These objects could exhibit OH maser emission from the neutral region, as well as radio continuum emission from the inner ionized envelope. Therefore, they would show characteristics of both standard OH/IR stars (strong infrared emission together with OH maser emission) and PNe (radio continuum emission at centimeter wavelengths). These peculiar sources are called OHPNe (Zijlstra et al. 1989).

This rare type of source probably represents an evolutionary phase immediately before the formation of a full-blown PN (Zijlstra et al. 1989). Therefore these sources are potentially key objects for studying the early evolution of PNe. García-Hernández et al. (2007) propose that strongly obscured OHPNe represent the population of high-mass precursors of PNe in our Galaxy. Given their potential interest in studying the early phases of PN evolution, it is important to have an updated and reliable catalog of OHPNe in order to study their characteristics and the possible relationship with other maser-emitting evolved objects.

Send offprint requests to: L. Uscanga

* present address: Universidade de Vigo

The seminal work by Zijlstra et al. (1989) cataloged 12 possible OHPNe. These were identified using three tools: (1) radio continuum observations of evolved stars with reported OH emission, (2) OH observations of possible young PNe, and (3) correlations between the OH and PN catalogs. However, as these authors point out, in several of those 12 identified candidates, the association between OH maser and radio continuum could not be confirmed, owing to the low positional accuracy of the data. Only in four of these objects had the positions of OH maser emission been measured with interferometric observations at that time. In the rest of the sources, the OH maser data were obtained in single-dish observations with beams of several arcminutes, so it is hard to ascertain whether the maser emission arises from the same source that shows radio continuum emission. In fact, in two of the sources cataloged by Zijlstra et al. (1989), new interferometric observations by Gómez et al. (2008) show that the reported continuum and OH maser emission were not associated with each other, therefore their classification as OHPNe should be revised.

After the publication by Zijlstra et al. (1989), new interferometric observations of radio continuum and OH masers toward evolved stars have been carried out, including large-scale surveys, e.g., the NRAO VLA Sky Survey (NVSS) (Condon et al. 1998) and the ATCA/VLA OH 1612 MHz survey (Sevenster et al. 1997a,b, 2001). Therefore, it is now possible to update the catalog of OHPNe, confirming the possible candidates with the current available radio-continuum and OH maser data of interferometric observations, which provide sufficient positional accuracy to associate these emissions.

Another important aspect to consider is the actual nature of these sources. We note that the observational definition of OHPNe as sources with both radio continuum and OH maser emissions (Zijlstra et al. 1989) may include sources that are not really PNe, so labeling them collectively as OHPNe may be misleading. There are evolved stars that show radio continuum emission and OH maser emission but are not PNe, such as symbiotic systems (Kafatos et al. 1989; Aaquist & Kwok 1990; Ivison et al. 1994), in which the envelope of a red giant is ionized by a hot companion (e.g., a white dwarf) or post-AGB stars (Bains et al. 2009) still too cold to ionize their envelopes but that may show radio continuum emission arising from shocks. If we want to study OHPNe in the context of the early evolution of PNe, it is important to distinguish between different types of OH and radio continuum emitters. In this paper, we reserve the term OHPNe for bona fide PNe only (objects in which photoionization from the central star has started), separating them from other evolved objects with OH maser and radio continuum emission.

In this work we present an updated list of OHPNe, with a study on their nature and characteristics. This paper is organized as follows. In Sect. 2 we describe the analysis of radio interferometric archival data of both radio continuum and OH maser emission. In Sect. 3 we describe the results obtained, including a description of confirmed sources, possible candidates, misclassified sources as OHPNe, and related objects. In Sect. 4 we summarize the general characteristics of the OHPNe sources. In Sect. 5 we present a brief discussion, and finally, in Sect. 6 we give our main conclusions.

2. Description of the analysis of radio interferometric data

2.1. Archival data of cataloged OHPNe

We retrieved and processed radio continuum and OH maser data from the 12 candidate OHPN reported by Zijlstra et al. (1989) that were available in the Very Large Array archive of the National Radio Astronomy Observatory (NRAO)¹. Our goal was to confirm the association between maser and radio continuum emission in those candidate sources. A list of the archival data used is given in Table 1.

VLA continuum and OH line data were calibrated and processed using the Astronomical Image Processing System (AIPS) package of NRAO, following standard procedures. Some data presented here have been previously published (Pottasch et al. 1987; Pottasch et al. 1988; Zijlstra et al. 1989; Ratag et al. 1990). However, our new data reduction includes the use of the robust scheme of visibility weighting (Briggs 1995), not available at the time of the original publications. We used a ROBUST parameter equals 0, as implemented in task IMAGR of AIPS, since it optimizes the trade-off between angular resolution and point-source sensitivity. Positions of continuum and OH emission were obtained by fitting elliptical Gaussians with task JMFIT. Unless stated otherwise, the positions given in this paper are those obtained in our reanalysis of data.

2.2. Literature search for new candidates

To find new OHPN candidate objects, additional to the ones reported by Zijlstra et al. (1989), we consulted the literature searching for interferometric data of both radio continuum and OH masers in PNe, identifying coincidences between their positions.

Positional information on the radio continuum emission was retrieved from published catalogs of optically identified PNe with radio continuum counterparts detected in large-scale interferometric surveys. In particular, we used the list of NVSS radio continuum detections (Condon & Kaplan 1998) coincident with sources in the Strasbourg-ESO Catalog of Galactic Planetary Nebulae (Acker et al. 1992), and in subsequent optical surveys (Luo et al. 2005). Furthermore, we used the PNe from the new Macquarie/AAO/Strasbourg H α (MASH) catalog detected at centimeter wavelengths in the NVSS and the Molonglo Galactic Plane Survey (MGPS-2), reported by Bojčić et al. (2011). Other PNe with radio continuum observations reported elsewhere (Aaquist & Kwok 1990; Van de Steene & Pottasch 1993, 1995; Van de Steene & Jacoby 2001) were also included in our list.

For positional information on OH maser emission, we used the ATCA/VLA OH 1612 MHz survey (Sevenster et al. 1997a,b, 2001), and publications reporting interferometric OH observations on specific sources, compiled in the database of circumstellar OH masers of Engels et al. (2010), which is a very complete compilation of OH maser data in evolved stars. With the positions of radio-continuum emission associated with PNe and the accurate positions of OH masers provided by the interferometric observations and surveys mentioned above, we made cross-identifications to find possible new OHPNe.

¹ The National Radio Astronomy Observatory is a facility of the National Science Foundation operated under cooperative agreement by Associated Universities, Inc.

2.3. Cross-identification of radio continuum and maser emission

From both our literature search and our own analysis of VLA archive data, we compared the positions of the OH maser emission with those of the radio continuum, to ascertain in which sources those emissions are associated. In the case of resolved radio continuum emission, we consider them associated if the maser position is projected within the limits of the radio continuum. For unresolved emission, we consider that the radio continuum and maser emission are associated when their positions are compatible within their relative positional errors.

For nonsimultaneous radio continuum and OH maser observations, the relative errors are imposed by the absolute astrometric error of each observation. These errors are difficult to evaluate in an interferometric observation (especially when using positions from the literature), since they depend on a number of factors, such as the phase errors, the intrinsic positional error of the phase calibrator, the distance from the target source to that calibrator, or the accuracy in the measurements of baseline length. Typically, these errors could be around one tenth of the synthesized beam (Baudry & Neri 2001). In this paper we have conservatively assumed positional errors of one fifth of the synthesized beam, and are typically $< 3''$. In addition to these errors, intrinsic to interferometric observations, there is a positional uncertainty due to the noise in the images (Reid et al. 1988), which is $\sigma_n \simeq \frac{\theta}{2\text{snr}}$, where σ_n is the 1-sigma uncertainty due to noise, θ the synthesized beam, and snr the signal-to-noise ratio of the source. In our case, this error due to noise is always much smaller than the former component, so it is negligible in comparison.

However, we note that in some data sets used in this paper, there are simultaneous observations of OH masers and radio continuum at 18 cm. In those cases, the relative uncertainties are determined by the noise error alone (σ_n), since the other components of absolute errors are the same for maser and continuum images. Therefore, for these simultaneous observations, the relative positions can be measured with much higher accuracy.

3. Results

The result of our reduction of archival data was the confirmation of five objects as OHPNe, and the rejection of four of them, from the list of Zijlstra et al. (1989). The additional literature search yielded a confirmed OHPN (IRAS 19255+2123) and a possible one (IRAS 17168–3736).

3.1. Confirmed OHPNe

We consider as true OHPNe only those objects identified in the literature as PNe in which both the OH maser and the radio continuum emissions have been detected, and these emissions are associated with the criteria mentioned in Sect. 2.3. Evolved objects with associated OH and radio continuum, but not found to be PNe, are not considered in this category (presented as related objects in Sect. 3.4). We have confirmed a total of six OHPNe, which are listed in Table 2. In the following, we give a brief description of each source.

3.1.1. IRAS 17103–3702 (NGC 6302)

NGC 6302 is a well-known multipolar PN. The $H\alpha$ and [NII] images show a complex morphology, with ionized lobes extended roughly in the east-west direction and a dark lane cov-

ering the waist of the nebula (see Meaburn et al. 2005, and references therein). This source was listed by Zijlstra et al. (1989) as OHPN 1. The first simultaneous VLA observations of continuum emission and OH maser line at 1612 MHz in this PN were reported by Payne et al. (1988). These observations clearly show the association of the OH maser emission with the continuum emission (see Figure 4 of Payne et al. 1988), with the OH masers being projected against the resolved radio continuum. Since the continuum and maser observations were simultaneous and at close frequencies, this spatial association is highly reliable. The radio continuum map presents a bipolar morphology better shown at 6 cm (Gómez et al. 1989), although extending along the northeast-southwest direction, different from the one in the optical images. The OH maser spectrum is dominated by a single peak at $V_{\text{LSR}} \simeq -41 \text{ km s}^{-1}$ (Payne et al. 1988), blueshifted with respect to the velocity of the optical nebula (-31.4 km s^{-1} , Schneider et al. 1983). The spectrum could be the superposition of several velocity components, giving rise to a broad profile, with emission spanning $\gtrsim 20 \text{ km s}^{-1}$. Thereafter, Sevenster et al. (1997b) also detected this source in the ATCA/VLA OH 1612 MHz survey toward the galactic disk region, and Condon & Kaplan (1998) detected the radio continuum emission at 20 cm in the NVSS. These positions are separated by only $\simeq 2''$ (see Table 2), which is within their positional errors.

3.1.2. IRAS 17347–3139

This young PN is obscured at optical wavelengths, but shows a clear bipolar morphology in near-infrared images (de Gregorio-Monsalvo et al. 2004; Sahai et al. 2007). The lobes have a total extension of $\sim 4''$ and are separated by a dark equatorial lane. Recent mid-infrared images with VISIR/VLT reveal a multipolar structure, possibly indicating that the nebula has been shaped by precessing jets (Lagadec et al. 2011).

This source was listed by Zijlstra et al. (1989) as OHPN 5. The 6 cm continuum of this PN was first reported by Ratag et al. (1990) and OH maser emission by Zijlstra et al. (1989). A detailed study of the radio continuum emission from this source has been carried out by Gómez et al. (2005), who interpret it as arising from an expanding ionized nebula, with a dynamical age of $\sim 120 \text{ yr}$. Further high-angular resolution observations of continuum (at 0.7, 1.3, 3.6, and 18 cm) and OH maser emission at 1612 MHz with the VLA were carried out by Tafoya et al. (2009). The radio continuum emission has a bipolar morphology of $\sim 1''.5$ in size, coinciding with the lobes observed at near-infrared wavelengths. The OH maser emission shows a narrow single peak at $V_{\text{LSR}} = -70 \text{ km s}^{-1}$, which is spatially projected within the limits of the radio continuum. This confirms their association, especially considering that the OH and continuum data at 18 cm were obtained simultaneously. Some of the additional spectral features present in the single-dish OH spectra (Zijlstra et al. 1989) may actually arise from other sources in its neighborhood (Tafoya et al. 2009). The OH feature is blueshifted with respect to the systemic velocity, $\simeq -55 \text{ km s}^{-1}$, derived from interferometric CO observations (D. Tafoya, private communication).

We also note that water maser emission was observed within $\sim 0''.25$ from the center of this OHPN, its association being firmly established through simultaneous interferometric observations of water masers and radio continuum at 1.3 cm (de Gregorio-Monsalvo et al. 2004). The spatial distribution and radial velocities of the water masers are suggestive of a rotating and expanding maser ring that traces the innermost regions of a torus formed at the end of the AGB phase.

3.1.3. JaSt 23

Van de Steene & Jacoby (2001) detected radio continuum emission at 3 and 6 cm toward this source using ATCA (Table 2). The position of this continuum source is offset $\approx 32''$ from IRAS 17371–2747, while the positional error of the IRAS source is $26''$. Therefore, it is possible that this continuum source is not associated with IRAS 17371–2747, as previously assumed by Zijlstra et al. (1989), who labeled it as OHPN 6. The cataloged IRAS source may in fact be the superposition of two different sources that are unresolved by IRAS (angular resolution $\approx 1' - 4'$), but distinct in WISE images: JaSt 23 (whose counterpart is likely to be WISE J174023.06-274911.7) and another reddened object (WISE J174018.10-274849.3), separated by $\approx 70''$. The position of the radio continuum coincides with that of the PN JaSt 23 (Jacoby & Van de Steene 2004). We also note that the continuum sources reported by Van de Steene & Jacoby (2001) and Zijlstra et al. (1989) are separated by more than $1'$, and we could only confirm the former in our data reprocessing. The OH maser emission at 1612 MHz of this source was detected in the ATCA/VLA survey toward the Galactic bulge region by Sevenster et al. (1997a). The OH maser spectrum shows a single peak at $V_{\text{LSR}} = +115.2 \text{ km s}^{-1}$, with a broad profile (width $\approx 15 \text{ km s}^{-1}$). The separation between the OH maser and continuum emissions is only $\sim 0''.9$ (Table 2). Considering the positional uncertainties, the OH maser and continuum emissions seem to be associated. The systemic velocity is still unknown.

3.1.4. IRAS 17393–2727

An HST image of IRAS 17393–2727 shows a highly collimated bipolar outflow, as well as a dark lane that completely obscures the central source (Manteiga et al. 2011). The infrared spectrum of this source shows bright [Ne II] nebular emission, strongly suggesting that the ionization of its central region has already started (García-Hernández et al. 2007).

This source was listed by Zijlstra et al. (1989) as OHPN 9. The radio continuum emission toward this source was detected at 2 and 6 cm using the VLA by Pottasch et al. (1987). The OH maser line at 1612 MHz was observed by Zijlstra et al. (1989) also with the VLA. We have confirmed the positions of both emissions in our reprocessing of VLA data archive, as well as OH maser emission at 1665 MHz. Moreover, Sevenster et al. (1997a) detected this source in the ATCA/VLA survey toward the Galactic bulge region. The OH spectrum at 1612 MHz shows a highly asymmetrical double peak, with features located at $V_{\text{LSR}} = -122.8 \text{ km s}^{-1}$ and -93.6 km s^{-1} , and intensity ratio (blueshifted/redshifted) of ≈ 70 . The positions of the OH maser and the radio-continuum emissions are separated $\sim 0''.3$, and are compatible within the errors (Table 2).

3.1.5. IRAS 19219+0947 (Vy 2–2)

Sahai et al. (2011) classified this source as an irregular PN, based on an HST $\text{H}\alpha$ image that shows extended emission but no obvious structure. Analysis of the internal kinematics (Miranda & Solf 1991) shows that Vy 2–2 consists of a slow expanding, compact central region ($\approx 0''.35$) and two rather wide bipolar features ($\geq 0''.6$). This is consistent with an elliptical/bipolar PN and with the structures observed in radio continuum (see below).

This source was listed by Zijlstra et al. (1989) as OHPN 12. Vy 2–2 is the first PN where OH maser emission was detected with single-dish observations (Davis et al. 1979).

Seaquist & Davis (1983) detected radio continuum (at 2, 6, and 20 cm) and OH (1612 MHz) maser emission with the VLA toward this source. Moreover, OH maser emission at 6035 MHz was detected toward this source with single-dish observations (Jewell et al. 1985; Desmurs et al. 2002, 2010). However, interferometric observations would be necessary to confirm its association with Vy 2–2. The VLA radio continuum map at 6 cm shows a slight elongation in the northeast-southwest direction (Seaquist & Davis 1983; Christianto & Seaquist 1998). However, at 1.3 cm (Seaquist 1991) and 2 cm (Seaquist & Davis 1983), it has a clear shell-like structure, with a diameter of $\approx 0.4''$. The radio continuum emission of this source was also detected in the NVSS (Condon & Kaplan 1998). The OH maser spectrum shows a single peak at $V_{\text{LSR}} \approx -62 \text{ km s}^{-1}$ with an asymmetrical profile spanning $\geq 8 \text{ km s}^{-1}$, which is blueshifted with respect to the velocity of the optical nebula (-53.4 km s^{-1} , Miranda & Solf 1991). The spatio-kinematical distribution of the OH maser emission is also consistent with an expanding shell (Shepherd et al. 1990), with the same center as the one seen in radio continuum. The distance between the peak of the continuum emission at 20 cm and the OH masers is only $\sim 0''.25$ (within the observational errors, Table 2). Moreover, the peak of the maser emission is projected against resolved structures traced by the radio continuum at 1.3, 2, and 6 cm (Seaquist & Davis 1983; Seaquist 1991), clearly indicating that these emissions are associated.

3.1.6. IRAS 19255+2123 (K 3–35)

K 3–35 is a young PN that shows a bipolar morphology in both optical images (Miranda et al. 2000) and VLA radio continuum maps at 2, 3.6, and 6 cm (Aaquist & Kwok 1989; Miranda et al. 2001). This continuum source was also detected in the NVSS at 20 cm (Condon & Kaplan 1998). The radio continuum emission exhibits a bright core and two bipolar lobes with an S-shape, which can be explained by a precessing jet evolving in a dense circumstellar medium (Velázquez et al. 2007).

The OH emission at 1612, 1665, 1667, and 1720 MHz (Aaquist 1993; Miranda et al. 2001; Gómez et al. 2009) is projected against the radio continuum structure, supporting the association of these emissions. Moreover, the OH maser emission at 1665 MHz arises within $\approx 0''.04$ from the peak of the radio continuum. The spectrum of the OH maser emission at 1612 MHz shows at least four features at $V_{\text{LSR}} \approx -2.0, +8.8$ (the brightest one), $+18.4, +21.2 \text{ km s}^{-1}$. The systemic velocity of this source is not well known: while the velocity of the optical nebula is $\approx 10 \text{ km s}^{-1}$ (Miranda et al. 2000), the velocity of the CO molecular gas is $\approx 25 \text{ km s}^{-1}$ (Tafoya et al. 2007). Interestingly, OH maser emission at 6035 MHz from this source has been recently confirmed with interferometric observations (Desmurs et al. 2010). This emission is very compact and located close in angular separation and velocity to the 1720 MHz maser line (Gómez et al. 2009). This is the only young PN where the maser lines at 6035 and 1720 MHz have been confirmed until now.

In the VLA observations carried out by Miranda et al. (2001), H_2O maser emission was also detected, within a region of $\approx 0''.025$ from the peak of the radio continuum emission, as well as in two regions at the tips of the bipolar radio jet $\approx 1''$ from the center. This was the first PNe in which H_2O maser emission was confirmed. The kinematics of the water masers from the central region suggests there is an expanding and rotating disk, almost oriented perpendicular to the innermost region of the ob-

served jet, which may be related with the collimation mechanism (Uscanga et al. 2008).

3.2. Possible OHPNe

In this category, on the one hand, we include sources in which the detection of OH maser emission has been carried out only with single-dish observations, and therefore, interferometric observations are needed to confirm the positional association with the radio continuum emission of the source. On the other hand, we also consider those sources here in which there is a confirmed association between maser and continuum emission, but their nature as PNe has not yet been determined. Possible OHPNe are listed in Table 3.

3.2.1. IRAS 17150–3754

This source was listed by Zijlstra et al. (1989) as OHPN 2. The radio continuum emission of this source was observed at 2 and 6 cm with VLA by Pottasch et al. (1987). The OH maser emission at 1612 MHz was first detected in single-dish observations using the Parkes antenna (Caswell et al. 1981), and later Zijlstra et al. (1989) confirmed that detection using the VLA, only $\sim 1''$ away from the continuum emission. Our reanalysis of the VLA archive data confirms the association of the OH and continuum positions (Table 3). We have found that the OH spectrum at 1612 MHz shows a double peak, with features located at $V_{\text{LSR}} \simeq -108.4 \text{ km s}^{-1}$ and -103.4 km s^{-1} and similar flux densities ($\simeq 280$ and 260 mJy , respectively). It is listed as a possible PN in the Strasbourg-ESO catalog (Acker et al. 1992), but its nature has not yet been confirmed.

3.2.2. IRAS 17168–3736

This source is not listed in the OHPN catalog by Zijlstra et al. (1989), but it is considered as an OHPN by García-Hernández et al. (2007). The radio continuum emission of this source was observed at 20 cm with the VLA by White, Becker, & Helfand (2005), although it is not listed in their published catalog. García-Hernández et al. (2007) refer to a radio continuum position in the online version of the MAGPIS catalog (Helfand et al. 2006). We also downloaded the corresponding image from the MAGPIS catalog at 20 cm and confirm there is a radio continuum source at the position given in Table 3.

The OH maser emission was first detected in single-dish observations using the Parkes antenna (Caswell et al. 1981) and later, Sevenster et al. (1997a) determined a more accurate interferometric position of the maser emission at 1612 MHz, only $2''.8$ away from the continuum emission, both positions coinciding within the errors (Table 3). The OH maser spectrum shows a double peak, with one feature located at $V_{\text{LSR}} = -19.1 \text{ km s}^{-1}$ and the other at $+7.2 \text{ km s}^{-1}$. The intensity ratio (blueshifted/redshifted) is about $\simeq 1.2$. This spectrum is similar to the one typically found in AGB stars. The nature of this source is still uncertain.

3.2.3. IRAS 17221–3038

This source was listed by Zijlstra et al. (1989) as OHPN 4. The radio continuum emission of this source at 6 cm was detected by Pottasch et al. (1988). We have confirmed this position in the review of the VLA archive data (Table 3). This source was also

detected at 20 cm in the NVSS (Condon & Kaplan 1998). On the other hand, the reported OH maser emission at 1612 MHz has been detected with the Nançay antenna (Zijlstra et al. 1989), and shows a double peak with features separated $\simeq 33 \text{ km s}^{-1}$. Unfortunately, the available VLA archive data in this source at 1612 MHz does not show any OH emission, since the velocity range covered by these interferometric observations did not include the OH features detected with the single-dish observations.

3.2.4. IRAS 17375–2759

This source is listed by Acker et al. (1992) as a possible PN and by Zijlstra et al. (1989) as OHPN 7. The radio continuum emission from this source was detected at 6 cm with interferometric observations by Pottasch et al. (1988). OH maser emission at 1612 MHz was detected in the ATCA/VLA survey toward the Galactic bulge region (Sevenster et al. 1997a), only $0''.7$ away from this continuum emission (Table 3). Therefore both emissions are associated considering the positional errors. The spectrum of the 1612 MHz OH line shows a double peak, with the spectral features at $V_{\text{LSR}} = +23.2 \text{ km s}^{-1}$ and $+30.5 \text{ km s}^{-1}$, and intensity ratio (blueshifted/redshifted) of $\simeq 3$. The nature of this source is still uncertain.

3.3. Sources previously misclassified as OHPNe

3.3.1. IRAS 17207–2856

This source was listed by Zijlstra et al. (1989) as OHPN 3. Pottasch et al. (1988) reported radio continuum emission with a flux density of 8.2 mJy at 6 cm. However, in our analysis of archival data, we did not detect any emission either at 3.6 or 6 cm, with upper limits of $\simeq 0.16 \text{ mJy beam}^{-1}$ (3σ) in both cases. There is no radio continuum source at 20 cm in the NVSS catalog (3σ upper limit $\simeq 1.4 \text{ mJy beam}^{-1}$). Moreover, we could not confirm the presence of maser emission associated with this source in the VLA data archive, consistent with the VLA non-detection mentioned by Zijlstra et al. (1989). This source had been classified as an OHPN based on a single-dish detection of OH maser emission with the Parkes antenna (Zijlstra et al. 1989), but it may arise from a different source. In either case, the absence of radio continuum emission allows us to reject it as an OHPN (see Table 4).

3.3.2. IRAS 17375–3000

This source was listed by Zijlstra et al. (1989) as OHPN 8. OH maser emission toward this source at 1612 MHz was detected with interferometric observations in the ACTA/VLA survey by Sevenster et al. (1997a). Its position is listed in Table 4. The OH maser spectrum shows a double peak, with features located at $V_{\text{LSR}} = -35.2 \text{ km s}^{-1}$ and -16.2 km s^{-1} . Radio continuum emission from this source could not be confirmed in our reanalysis of two independent data sets from the VLA archive. Moreover, the radio continuum source reported by Ratag et al. (1990) is $\simeq 20''$ away from the position of the OH maser. Considering that the beam of the radio continuum observations of Ratag et al. (1990) ranged between $\simeq 5''$ and $10''$, and therefore, the absolute positional uncertainty should be $\lesssim 2''$, we think it is unlikely that the OH maser (with a positional error $\simeq 2''.4$) is associated with the reported continuum source, even if the latter is real.

3.3.3. IRAS 17418–2713

This source was considered as an OHPN by García-Hernández et al. (2007), but it is not listed in the catalog of Zijlstra et al. (1989). However, the radio continuum emission at 6 cm toward this source reported by Ratag & Pottasch (1991) is located $17''$ away from the OH maser emission observed at 1612 MHz in the ACTA/VLA survey by Sevenster et al. (1997a). Its position is listed in Table 4. The OH maser spectrum shows a double peak, with features located at $V_{\text{LSR}} = -27.9 \text{ km s}^{-1}$ and $+2.8 \text{ km s}^{-1}$. The beam size of the radio continuum observations was $\approx 35''$, and therefore the absolute positional uncertainty should be $\lesssim 7''$. Considering that the position error of the OH maser is $\approx 2''.4$, we conclude that it is not associated with the radio continuum emission reported by Ratag & Pottasch (1991). In our reanalysis of VLA data we have found no radio continuum emission that may be associated with the OH maser.

Based on the infrared spectrum of this source that shows strong amorphous silicate absorption features, together with high variability, García-Hernández et al. (2007) point out that this source may still in the AGB phase, which also strongly suggests that this source is not an OHPN.

3.3.4. IRAS 17443–2949

This source was listed by Zijlstra et al. (1989) as OHPN 10. Radio continuum emission toward this source was reported with the VLA by Ratag et al. (1990), while single-dish observations showed OH maser emission at 1612 MHz (Zijlstra et al. 1989). However, Gómez et al. (2008) carried out simultaneous radio continuum and OH maser observations toward this source. They detected both OH 1612 and 1665 MHz lines, but no radio continuum, either at 1.3 or 18 cm (Table 4). No radio continuum emission was present in our reanalysis of the available archival VLA data. In any case, the radio continuum at 6 cm reported by Ratag et al. (1990) is $\sim 10''$ away from the position of the OH masers. Since this separation is larger than the positional uncertainty ($\approx 3''$), we consider that the OH maser is not associated with the radio continuum emission, even if the latter was real.

Moreover, Gómez et al. (2008) detected H_2O maser emission associated with IRAS 17443–2949 located very close to the OH maser components but also $\sim 9''$ away from the radio continuum source reported by Ratag et al. (1990). On the other hand, García-Hernández et al. (2007) suggest that this source is still in the AGB phase. Based on its AGB nature, the detection of OH and H_2O maser emission (the latter very rarely found in PNe), and its unlikely association with the radio continuum emission, Gómez et al. (2008) classified this source as an OH/IR star.

3.3.5. IRAS 17580–3111

This source was listed by Zijlstra et al. (1989) as OHPN 11. Ratag et al. (1990) reported radio continuum emission at 6 cm toward this source. OH maser emission at 1612 MHz was detected by Zijlstra et al. (1989) in single-dish observations, showing at least four spectral components. With interferometric VLA observations, Gómez et al. (2008) detected OH maser emission at 1612 MHz with a typical double-peaked spectrum, but radio continuum emission was not detected at either 1.3 or 18 cm (Table 4). We could not detect any radio continuum emission in the available VLA archival data. The position of the OH maser emission (with an uncertainty of $\approx 3''$) is $57''$ away from the ra-

dio continuum source reported by Ratag et al. (1990), so is not associated with it, even if the latter is real.

In addition, Gómez et al. (2008) detected H_2O maser emission associated with this source. García-Hernández et al. (2007) classified IRAS 17580–3111 as a post-AGB star, based on its infrared spectrum and its low variability.

3.4. Related objects

We have found other evolved objects that fulfill the observational characteristics for being considered as OHPNe (showing both radio continuum and OH maser emission), but they are not PNe: e.g., symbiotic binary systems or post-AGB stars. Since our focus in this paper is to search for true OHPNe, we have not carried out an extensive search for these other objects. However, we mention a few of them, to illustrate the importance of characterizing the nature of evolved objects for a proper classification as OHPNe. We also include them in the next sections, to compare their characteristics with those of bona fide OHPNe.

Two symbiotic systems are among the related objects: IRAS 17463–3700 (Aaquist & Kwok 1990; Ivison et al. 1994) and IRAS 23412–1533 (R Aqr) (Kafatos et al. 1989; Ivison et al. 1994), as well as some post-AGB stars, such as IRAS 15367–5420, IRAS 15445–5449, and IRAS 16372–4808, where the radio continuum and OH maser emissions are strongly associated, but in these sources the continuum emission may be arising from shocks since the central stars are still too cold to ionize their envelopes (Bains et al. 2009). Particularly, in IRAS 15445–5449 water maser emission was detected with single-dish (Deacon et al. 2007) and interferometric observations (Pérez-Sánchez et al. 2011), with a wide velocity spread. Therefore, this source is a “water fountain”, a type of object showing an early manifestation of collimated mass loss in evolved stars (Imai 2007). We have included this interesting source in the following sections, for its relevance in the evolutionary scheme of intermediate-mass stars.

4. General characteristics of OHPNe

Here we discuss some observational properties of the confirmed OHPNe sources, comparing them with those of possible OHPNe and related objects. We think that these observational characteristics can be useful for future studies of these types of objects, especially when more of them have been detected.

4.1. Morphology

All OHPNe for which the ionized emission has been resolved, present a bipolar morphology at optical, infrared and/or radio wavelengths. This is less clear in the case of IRAS 19219+0947 (Vy 2–2) for which the HST images show an irregular morphology (Sahai et al. 2011), although the internal kinematics do indicate the presence of bipolar mass motions (Miranda & Solf 1991). These bipolar morphologies suggest that OH maser emission in PNe is related to nonspherical mass-loss phenomena, rather than being the remnant of the masers excited in the spherical AGB wind. There is no resolved image of the OHPN JaSt 23 and the four OHPN candidates (IRAS 17150–3702, IRAS 17168–3736, IRAS 17221–3038, and IRAS 17375–2759).

Regarding the related objects, the symbiotic systems IRAS 17463–3700 and IRAS 23412–1533 seem to show an elongated structure at radio wavelengths (Kafatos et al. 1989). Moreover IRAS 23412–1533 (R Aqr) presents a clear bipolar morphology

in optical images (Paresce & Hack 1994). The “water fountain” post-AGB star IRAS 15445–5449 shows a bipolar structure with a dark lane in mid-infrared images (Lagadec et al. 2011).

4.2. Infrared colors

In Figure 1, we present the IRAS two-color diagram of the confirmed OHPNe and related objects. The IRAS colors are defined in the classical way as $[a] - [b] = -2.5 \log(S_a/S_b)$, where S is the flux density at wavelengths a and b (in μm). This diagram shows that all the confirmed OHPNe present a value of $[12] - [25] > 1.0$, which is typical of PNe (van der Veen & Habing 1988), more specifically between ≈ 1.75 and 2.75 . The values of the $[25] - [60]$ show a higher dispersion. The possible OHPNe present similar values for the $[12] - [25]$ color. The far infrared colors of the symbiotic systems IRAS 17463–3700 and IRAS 23412–1533 clearly differ from those of bona fide OHPN. They are located in a region of the diagram commonly populated by variable stars with young oxygen-rich circumstellar shells and AGB stars (van der Veen & Habing 1988). Therefore, their infrared emission seem to be dominated by the red giant companion.

In Figure 2, we show the position in the $[8]-[12]$ vs $[15]-[21]$ two-color diagram of the confirmed OHPN sources and related objects that have been observed with the Midcourse Space Experiment (MSX) satellite. Sevenster (2002) defined four quadrants in this diagram, each of which tends to be populated by a different type of star. Quadrants QI to QIV tend to correspond with late post-AGB stars, star-forming regions, AGB stars, and early post-AGB stars, in that order. Although this diagram cannot be used to ascertain the nature of a particular source (e.g., post-AGB stars and PNe can be found in QII and QIII, see Suárez 2004), it is useful to see overall evolutionary trends.

Confirmed and possible OHPNe are mostly located in QI, consistent with their proposed nature as young PNe. IRAS 17103–3702 and IRAS 19219+0947, well-known PNe, are in QII, although relatively close to the boundary. Their location may suggest a differential characteristic with respect to the rest of sources, such as being in a more evolved stage. On the other hand, the location of the candidate IRAS 17168–3736 in QIV is well separated from the rest of sources, which casts some doubt on its nature as an OHPN.

As a comparison, the symbiotic star IRAS 17463–3700 is located in QIII, also well-separated from the main group of OHPNe. Its location in QIII is consistent with the infrared emission being dominated by the red giant component of the system. The post-AGB star IRAS 15445–5449 has colors similar to those of OHPNe, although it has a higher value of $[8]-[12]$.

4.3. Spectral energy distributions

We searched the Two Micron All Sky Survey (2MASS), Deep Near Infrared Survey of the Southern Sky (DENIS), MSX, IRAS, AKARI, Spitzer, Wide-field Infrared Survey Explorer (WISE), and Infrared Space Observatory (ISO) databases for infrared photometric and spectroscopic data that could be used to construct the spectral energy distributions (SEDs) of these objects. Combined data from these catalogs cover the spectral region from ≈ 1 to $100 \mu\text{m}$. The SEDs were constructed with these infrared data, together with the available measurements of the radio continuum emission.

Figure 3 shows the SEDs of the confirmed OHPNe. All show a clear peak at $\approx 25 \mu\text{m}$ (although the SED of JaSt 23 is not well

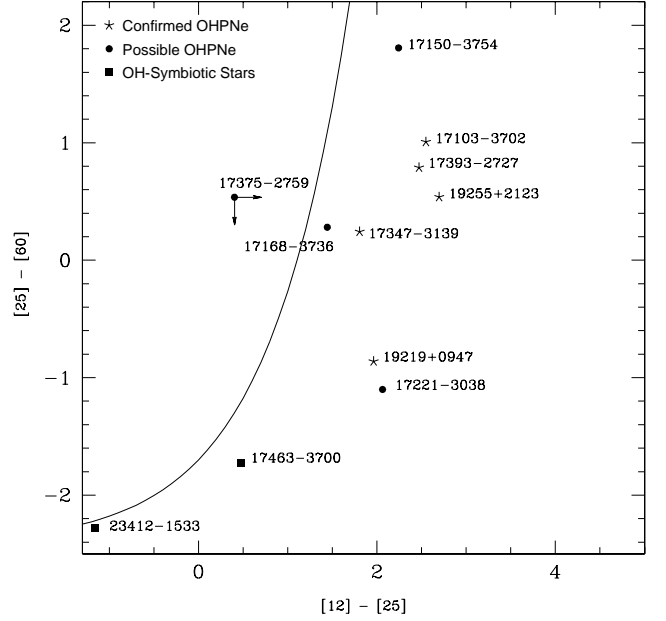


Fig. 1. IRAS two-color diagram with the position of the confirmed and possible OHPNe, as well as of related objects, with which IRAS data could be associated. Asterisks represent the confirmed OHPNe, circles are the candidate OHPNe, and squares are symbiotic stars. The solid line is the curve modeled by Bedijn (1987) showing the location of AGB stars.

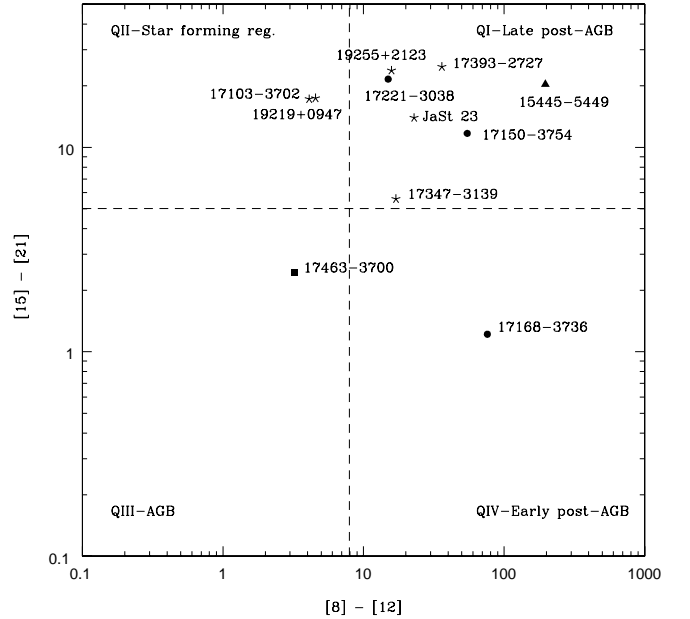


Fig. 2. MSX two-color diagram with the position of the confirmed and possible OHPNe and related objects for which MSX data are available. The vertical and horizontal lines divide the diagram into four quadrants that correspond to the areas of higher probability of containing the different types of objects labeled on the diagram (Sevenster 2002). The symbols have the same meaning as in Fig. 1. The triangle represents the “water fountain” post-AGB star IRAS 15445–5449.

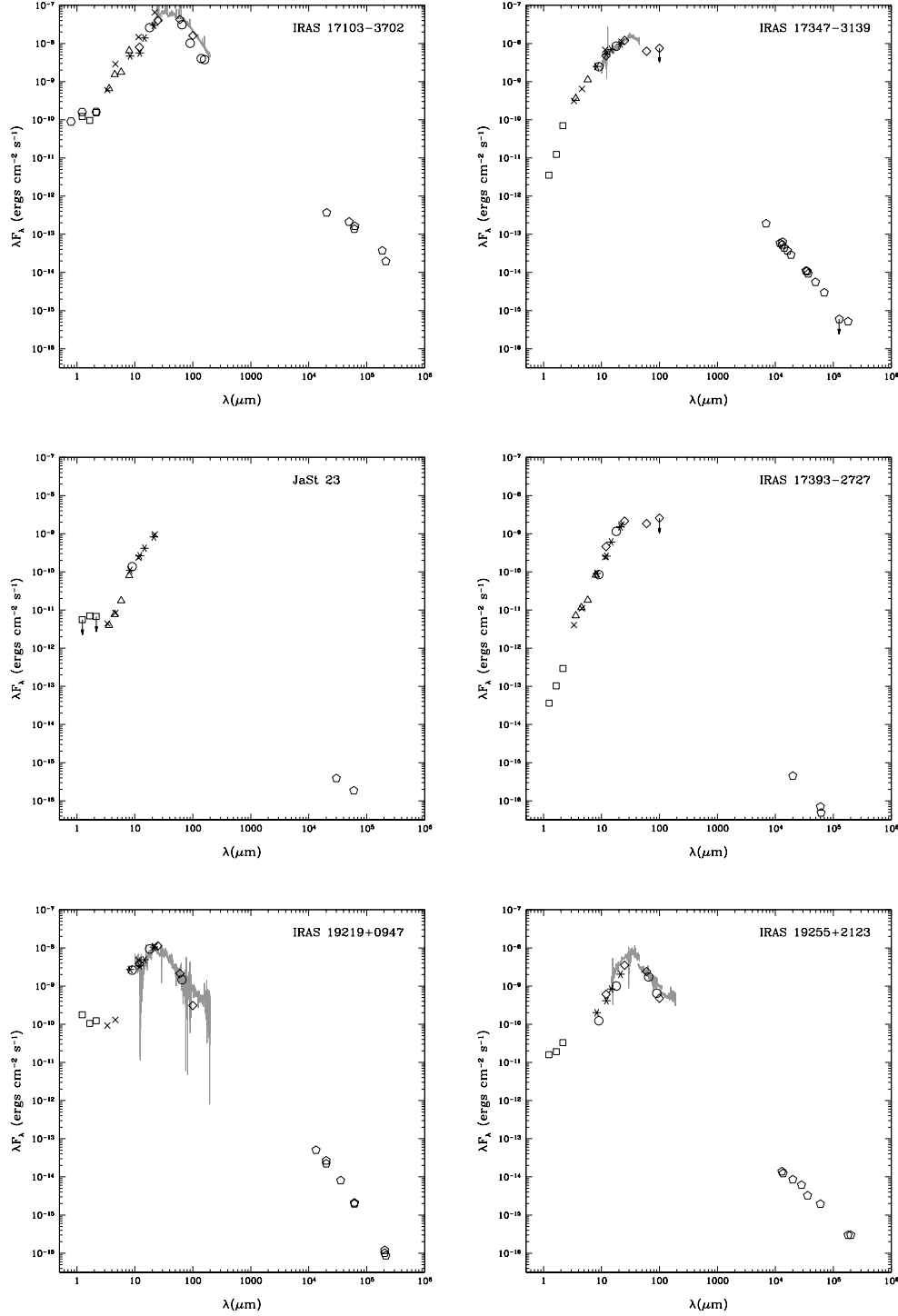


Fig. 3. SEDs of the confirmed OHPNe. The hexagons, squares, triangles, crosses, asterisks, circles, and diamonds represent the DENIS, 2MASS, Spitzer, WISE, MSX, Akari, and IRAS data, respectively. The pentagons represent measurements at different radio wavelengths. The ISO spectrum is shown in gray when available. The arrows indicate an upper limit value. The flux densities of radio continuum in the different sources were measured by the following authors: IRAS 17103–3702 (Rodríguez et al. 1985; Payne et al. 1988), 17347–3139 (Gómez et al. 2005; Tafoya et al. 2009), JaSt23 (Van de Steene & Jacoby 2001), IRAS 17393–2727 (Pottasch et al. 1987, this paper), IRAS 19219–0947 (Seaquist & Davis 1983; Christianto & Seaquist 1998; Condon & Kaplan 1998), and IRAS 19255+2123 (Aaquist & Kwok 1991; Miranda et al. 2001; Gómez et al. 2009). The Spitzer fluxes for IRAS 17103–3702 (triangles) and J, H, K fluxes (squares) for IRAS 17393–2727 were measured by Phillips & Ramos-Larios (2008) and Ramos-Larios et al. (2012), respectively.

sampled at those wavelengths), tracing the dust in the circumstellar envelope. Moreover, in the sources IRAS 17103–3702,

IRAS 19219+0947, and JaSt 23, there is a hint that the emission flattens or rises again at $\lesssim 2 \mu\text{m}$, which could be the contri-

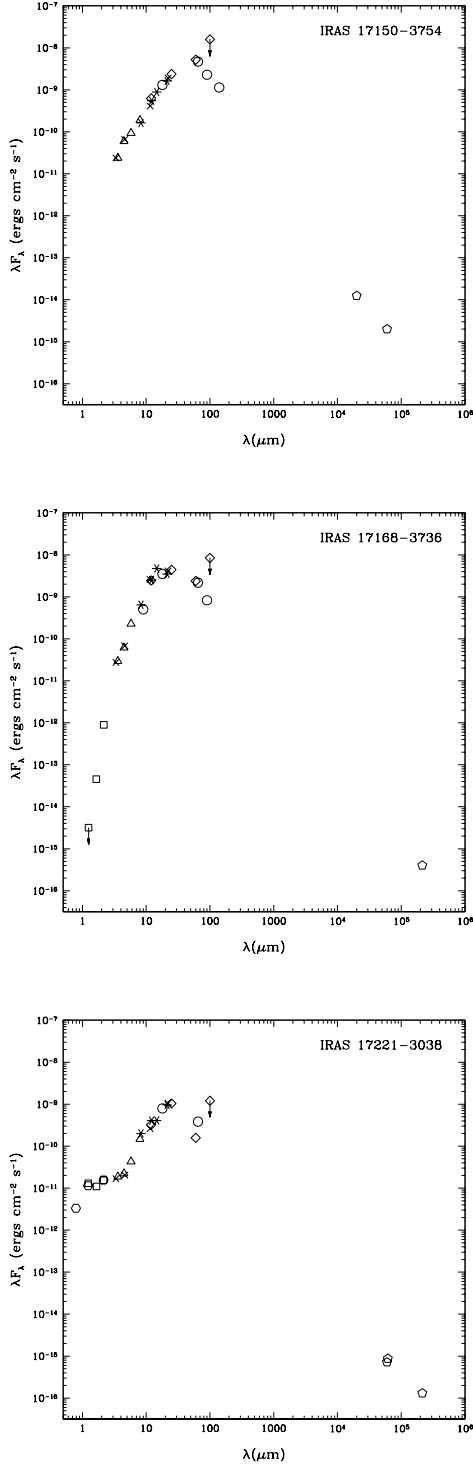


Fig. 4. SEDs of the possible OHPNe. Symbols mean the same as in Fig. 3. J, H, and K measurements taken by Ramos-Larios et al. (2012). The flux densities of radio continuum in the different sources were measured by the following authors: IRAS 17150–3754 (Pottasch et al. 1987), IRAS 17221–3038 (Pottasch et al. 1988; Condon & Kaplan 1998, this paper), and IRAS 17168–3736 (this paper).

bution from the central stellar component or free-free emission from the ionized nebula (Zhang & Kwok 1991). In contrast, the SEDs of IRAS 17347–3139 and IRAS 17393–2727 present a

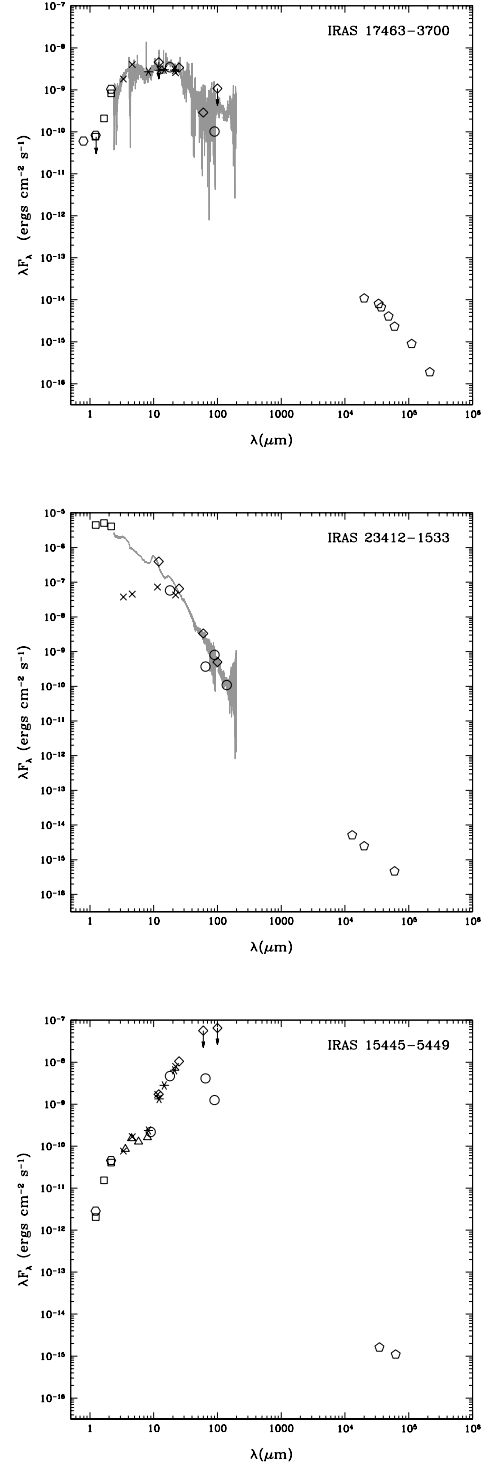


Fig. 5. SEDs of some of the related objects. Symbols mean the same as in Fig. 3. The ISO spectrum is shown in gray when available. The flux densities of radio continuum in the two sources were measured by the following authors: IRAS 17463–3700 (Purton et al. 1982; Aaquist & Kwok 1991; Condon & Kaplan 1998), IRAS 23412–1533 (Sopka et al. 1982), and IRAS 15445–5449 (Bains et al. 2009).

steep fall-off at $\lambda \lesssim 25 \mu\text{m}$, and a more gradual one in IRAS 19255+2123, but no sign of the emission rising at short wavelengths. In these sources, the circumstellar envelope may still

be optically thick, obscuring the stellar and ionized component. They could be comparatively younger than IRAS 17103–3702, IRAS 19219+0947, and JaSt 23.

Figure 4 shows the SEDs of the candidate OHPNe. We did not present the SED for IRAS 17375–2759, since the infrared counterpart of the radio emission is uncertain. These candidate sources also show a maximum at $\geq 25 \mu\text{m}$. For the two sources that are well-sampled in the near infrared, we also see a dichotomy, with IRAS 17168–3736 showing a steep fall-off, while IRAS 17221–3038 seems to flatten at those wavelengths.

Finally, Figure 5 shows the SEDs of some related objects (symbiotic and post-AGB stars showing both radio continuum and OH maser emission). These SEDs are significantly different from those of the OHPNe, in their shape and the location of the maximum. It seems that the SED characteristics are useful for differentiating bona fide OHPNe from other OH-maser-emitting objects.

4.4. Spectral properties of OH masers

OH maser spectra in AGB stars typically present double-peaked profiles, with narrow components separated by $\sim 30 \text{ km s}^{-1}$, which have been interpreted as arising from the approaching and receding sides of the circumstellar envelope (Sevenster et al. 1997a). The peaks are sometimes asymmetrical, which could result in single-peaked profiles if one of the peaks is below the sensitivity of the instrument. However, the general trend is that the OH spectra are relatively symmetrical in those stars. Departures from the double or single-peaked profile are interpreted as tracing the departure from the nearly spherically symmetric mass loss of the AGB (Deacon et al. 2004).

We note that spectra of all the confirmed OHPNe show strong asymmetry, preferentially with blueshifted emission with respect to the stellar velocity. IRAS 17347–3139 and IRAS 17393–2727 show narrow blueshifted components, whose redshifted counterpart is absent or much weaker (almost by two orders of magnitude). IRAS 17103–3702, JaSt 23, and IRAS 19219+0947 also show blueshifted emission with a relatively wide component ($\geq 10 \text{ km s}^{-1}$), while OH components in AGB stars are typically narrower. IRAS 19255+2123 shows four OH features, two redshifted and two blueshifted, but the brightest of them is blueshifted, assuming that the systemic velocity is given by the velocity of the optical nebula. We note that the four OH maser features are blueshifted with respect to the velocity of the molecular gas traced by CO and HCO^+ , which is likely to arise from the circumstellar environment of the source (Tafoya et al. 2007). In all OHPNe, the OH spectra are different from the typical one in AGB stars. OHPN candidates also show strongly blueshifted and atypical spectra, with the exception of IRAS 17168–3736, which resembles an AGB spectrum. We note a possible observational bias, since one of the tools used by Zijlstra et al. (1989) to identify possible OHPNe was to search for radio continuum emission toward OH/IR stars whose redshifted OH emission was weak or absent. This criterion assumed that ionized gas could obscure OH emission in the background. However, among the sources in this paper, only the confirmed OHPN IRAS 17393–2727 and the candidate IRAS 17150–3754 were obtained with this observational bias. Therefore, the trend towards blueshifted spectra seems to be real and not an a priori bias. In fact, blueshifted spectra can be due to two independent effects produced by the radio continuum emission: absorption of the redshifted OH emission and/or amplification of the radio continuum emission by the gas in the foreground (leading to increased blueshifted emission).

The ionized gas in younger PNe tends to have larger emission measures (Kwok et al. 1981), which translates into higher opacities of the free-free continuum emission, especially at low frequencies. For instance, in the case of IRAS 17347–3139, Gómez et al. (2005) determine an emission measure of $\approx 1.5 \times 10^{-9} \text{ cm}^{-6} \text{ pc}$. With this value, the optical depth of the radio continuum emission at 1612 MHz would be ≈ 180 , and therefore the maser emission in the background would effectively be quenched. If the OH emission arises from an expanding envelope, this could explain a single blueshifted peak in this source.

In addition to that, the presence of radio continuum emission could itself enhance the blueshifted OH emission. Maser emission occurs when the populations of molecules in the gas are inverted due to large energy input (e.g., via shocks or radiation). Background radiation going through this gas with inverted populations stimulates the emission, and it is exponentially amplified in the process. In the case of AGB stars, the background radiation that is amplified in OH masers can be the cosmic background or intrinsic spontaneous emission in the envelope. This background emission is weak, and a long optical path along gas with inverted population is needed. However, the free-free radiation provides a stronger background emission that can be amplified, leading to observable OH emission from a gas that would not be present without the radio continuum. This effect would produce maser emission from the foreground (approaching) gas.

4.5. Relationship with H_2O maser-emitting PNe

Water maser observations have been carried out toward the six confirmed OHPNe. Nondetections toward IRAS 17103–3702, IRAS 17393–2727, IRAS 19219+0947, and JaSt 23 have been reported by Zuckerman & Lo (1987), Gómez et al. (1990), de Gregorio-Monsalvo et al. (2004), Deacon et al. (2007), and Suárez et al. (2007). On the other hand, detections of water masers have been confirmed through interferometric observations in IRAS 19255+2123 and IRAS 17347–3139 by Miranda et al. (2001) and de Gregorio-Monsalvo et al. (2004), respectively. These are two of the three H_2O -maser-emitting PNe confirmed to date. Interestingly, the third H_2O -PNe already reported, IRAS 18061–2505 did not present any OH maser emission (Gómez et al. 2008), while more recent observations of IRAS 17347–3139 show that the H_2O masers have disappeared (Suárez et al. 2007). In the case of the candidate OHPNe, IRAS 17150–3754 and IRAS 17168–3736 have also been observed, when searching for water maser emission, but nondetections were reported (Gómez et al. 1990; Deacon et al. 2007).

The presence of two objects in which masers from both species have been detected suggests a relationship between H_2O - and OH-emitting PNe. The relationship is also supported by the fact that PNe with either type of masers show bipolar morphologies (Miranda et al. 2010). It has been suggested that both H_2O -PNe and OHPNe originate in intermediate-mass stars, 5 to $8 M_{\odot}$ (Suárez et al. 2007; Pottasch & Bernard-Salas 2010). It is possible that H_2O -PNe and OHPNe belong to the same underlying type of objects or that there is an evolutionary trend, with H_2O -PNe being comparatively younger. However, given the still small number of confirmed PNe with either H_2O or OH masers and the variability of the maser emission, it is not possible to ascertain any such trend at this stage.

5. Discussion and future prospects

The confirmed OHPNe presented in this paper do not seem to constitute a homogeneous group, as they show significantly dif-

ferent characteristics. For example, IRAS 17347–3139 is optically obscured, and the PN JaSt 23 is very a compact source, suggesting that they are very young PNe. On the other hand, IRAS 17103–3702 and IRAS 19219+0947 show a complex structure in the optical, and they seem to be more evolved sources. In particular, IRAS 17103–3702 appears to be a full-blown PN. The different location in the MSX color-color diagram of these two sources (Figure 2) also suggests they have distinctive characteristics.

The presence or absence of different maser species has traditionally been proposed as a clock tracing different evolutionary stages (Lewis 1989; Gómez et al. 1990). In particular, masers were expected to sequentially disappear after the end of the AGB mass-loss, with timescales of ≈ 10 , 100, and 1000 yr for SiO, H₂O, and OH, respectively. This scheme implies that PNe showing OH maser emission must necessarily be very young. However, the existence of OHPNe in apparently different evolutionary stages suggests that this linear scheme of disappearance with time of the maser species may not be applicable. Thus, the presence of OH may depend on other parameters than age, such as the mass-loss rate of the object or the particular orientation of the nebula with respect to the line of sight.

The simple scheme of the sequential disappearance of masers is further challenged by the presence of water masers in “water fountain” post-AGB stars (Imai 2007), since these masers do not seem to be the remnants of the ones tracing the strong (and mostly spherical) mass loss in the AGB. In the case of water fountains, the masers trace highly collimated jets, which start in the late AGB or early post-AGB phase. In the case of PNe, the water masers pumped in the AGB are not expected to survive, given their short expected lifetimes (100 yr after the end of the AGB mass-loss), and yet water masers are present in PNe, which also indicate an excitation mechanism different from that in the AGB. Moreover, the existence of a PN with water masers (IRAS 18061–2505, Gómez et al. 2008), but without OH, does not easily fit a simple time-dependent scenario.

Suárez et al. (2009) propose an evolutionary scheme for water masers in evolved stars, in which this emission is first associated with the strong mass loss in the AGB, but when it ends, these masers can be excited by different processes, probably related to collimated mass loss in the post-AGB. These newly produced water masers would first trace jets (e.g. in water fountains) and disks in later stages (PNe). The case of OH masers could be different. As discussed in Sect. 4.4, the presence of radio continuum emission could produce OH masers in physical conditions that were insufficient to produce maser emission before ionization started. It is then possible that OH masers pumped in the AGB phase disappear during the post-AGB phase, but reappear once the source becomes a PN, and its radio continuum emission is amplified by the OH molecules. Therefore, OH maser emission could last significantly longer than 1000 yr after the end of the AGB, even assuming that the maser-emitting material is the remnant of the one excited during that phase. The presence of OH masers in PN would be favored in sources with bright radio continuum emission, and therefore they could last longer in PNe with more massive central stars, which ionize a larger amount of gas in the envelope.

With the results of this paper, only six confirmed OHPNe and four candidate OHPNe have been identified. Finding a larger number of OHPNe will be an important step toward a full understanding of the physical characteristics and evolution of these sources. This can be achieved with complete, sensitive, and unbiased surveys of radio continuum and OH masers. New instrumentation, such as ASKAP and APERTIF, are especially well-

suited to large-scales surveys of OH maser and radio continuum emission, since their implementation of focal plane arrays (which increase the instantaneous field of view of radio interferometers) will provide a huge improvement in survey speed. In particular, the results from ASKAP surveys EMU (Norris et al. 2011) in continuum and GASKAP (Dickey et al. 2012) in OH, will help us compile a much more complete catalog of OHPNe in our galaxy.

6. Summary

We have consulted the literature and public data archives, to obtain an updated catalog of OH-maser-emitting planetary nebulae (OHPNe), based on the spatial matching of sources found in interferometric observations of radio continuum and OH maser emission. Our main conclusions are as follows.

- We have found six objects, previously identified as PNe, which show both radio continuum and OH maser emission. These can be considered as bona fide OHPNe. Four additional objects are candidate OHPNe, still to be confirmed.
- All OHPNe for which the ionized emission has been resolved, present a bipolar morphology at optical, infrared, and/or radio wavelengths.
- The infrared colors of OHPNe are consistent, with most of them being young PNe.
- OH maser components in OHPNe tend to be blueshifted with respect to the systemic velocity. This could be due either to obscuration of the redshifted masers by optically thick radio continuum emission or to maser amplification of the radio continuum by the expanding gas closer to the observer.
- OHPNe do not form an homogeneous group. Their characteristics indicate that they may span a wide range of relative ages. We suggest that OH masers pumped in the AGB phase may disappear during the post-AGB phase, but reappear once the source becomes a PN, and its radio continuum emission is amplified by the OH molecules. Therefore, OH maser emission could last significantly longer than 1000 yr after the end of the AGB, with longer lifetimes in PNe with more massive central stars.

Acknowledgements. LU and JFG wish to express their gratitude for the help and hospitality provided by the staff at CSIRO Science and Space Science (Australia) during part of the preparation of this paper. This research has made use of the SIMBAD data base, operated at the CDS, Strasbourg, France, and the NASA/IPAC Infrared Science Archive, which is operated by the Jet Propulsion Laboratory, California Institute of Technology, under contract with the National Aeronautics and Space Administration. It makes use of data products from the Two Micron All Sky Survey (a joint project of the University of Massachusetts and the Infrared Processing and Analysis Center/California Institute of Technology, funded by NASA and NSF), DENIS (partly funded by the SCIENCE and the HCM plans of the European Commission under grants CT920791 and CT940627), Spitzer Space Telescope (operated by the Jet Propulsion Laboratory, California Institute of Technology under a contract with NASA), WISE (a joint project of the University of California, Los Angeles, and the Jet Propulsion Laboratory/California Institute of Technology, funded by NASA), AKARI (a JAXA project with the participation of ESA), and MSX (funded by the Ballistic Missile Defense Organization with additional support from NASA Office of Space Science). The authors acknowledge support from grants AYA2008-06189-C03-01 (JFG, OS, and LU) and AYA 2011-30228-C03-01 (JFG, LFM, and OS) of the Spanish Ministerio de Ciencia e Innovación (MICINN), cofunded by FEDER funds. LFM is also partially supported by grants INCITE09E1R312096ES and INCITE09312191PR of the Galician INCITE research program of the Dirección Xeral de Investigación, Desenvolvemento y Innovación of the Spanish Xunta de Galicia. JFG acknowledges partial support from grant TIC-126 of Consejería de Economía, Innovación y Ciencia of Junta de Andalucía.

References

- Aaquist, O. B. 1993, *A&A*, 267, 260
- Aaquist, O. B., & Kwok, S. 1989, *A&A*, 222, 227
- Aaquist, O. B., & Kwok, S. 1990, *A&AS*, 84, 229
- Aaquist, O. B., & Kwok, S. 1991, *ApJ*, 378, 599
- Acker, A., Marcout, J., Ochsenbein, F., Stenholm, B., & Tylenda, R. 1992, The Strasbourg-ESO Catalogue of Galactic Planetary Nebulae (Garching: European Southern Observatory)
- Bains, I., Cohen, M., Chapman, J. M., Deacon, R. M., & Redman, M. P. 2009, *MNRAS*, 397, 1386
- Baudry, A., & Neri, R. 2001, in *Millimeter Interferometry, Proceedings from the IRAM Millimeter Interferometry Summer School 2*, Ed. A. Dutrey, http://iram.fr/IRAMFR/IS/IS2002/html_2/book.html, 20
- Bedijn, P. J. 1987, *A&A*, 186, 136
- Blöcker, T. 1995, *A&A*, 299, 755
- Bojičić, I. S., Parker, Q. A., Filipović, M. D., & Frew, D. J. 2011, *MNRAS*, 412, 223
- Bowers, P. F., Johnston, K. J., & de Vegt, C. 1989, *ApJ*, 340, 479
- Briggs, D. S. 1995, PhD Thesis, New Mexico Institute of Mining and Technology
- Caswell, J. L., Haynes, R. F., Goss, W. M., & Mebold, U. 1981, *Australian Journal of Physics*, 34, 333
- Christiano, H., & Seaquist, E. R. 1998, *AJ*, 115, 2466
- Condon, J. J., Cotton, W. D., Greisen, E. W., et al. 1998, *AJ*, 115, 1693
- Condon, J. J., & Kaplan, D. L. 1998, *ApJS*, 117, 361
- Davis, L. E., Seaquist, E. R., & Purton, C. R. 1979, *ApJ*, 230, 434
- Deacon, R. M., Chapman, J. M., & Green, A. J. 2004, *ApJS*, 155, 595
- Deacon, R. M., Chapman, J. M., Green, A. J., & Sevenster, M. N. 2007, *ApJ*, 658, 1096
- de Gregorio-Monsalvo, I., Gómez, Y., Anglada, G., Cesaroni, R., Miranda, L. F., Gómez, J. F., & Torrelles, J. M. 2004, *ApJ*, 601, 921
- Desmurs, J.-F., Baudry, A., Sivagnanam, P., & Henkel, C. 2002, *A&A*, 394, 975
- Desmurs, J.-F., Baudry, A., Sivagnanam, P., et al. 2010, *A&A*, 520, A45
- Dickey, J. M., McClure-Griffiths, N., Gibson, S. J., et al. 2012, *PASA*, in press
- Engels, D., Bunzel, F., & Heidmann, B. 2010, *Database of Circumstellar Masers v 2.0*
- García-Hernández, D. A., Perea-Calderón, J. V., Bobrowsky, M., & García-Lario, P. 2007, *ApJ*, 666, L33
- Gómez, J. F., de Gregorio-Monsalvo, I., Lovell, J. E. J., Anglada, G., Miranda, L. F., Suárez, O., Torrelles, J. M., & Gómez, Y. 2005, *MNRAS*, 364, 738
- Gómez, Y., Moran, J. M., & Rodríguez, L. F. 1990, *Revista Mexicana de Astronomía y Astrofísica*, 20, 55
- Gómez, Y., Rodríguez, L. F., Moran, J. M., & Garay, G. 1989, *ApJ*, 345, 862
- Gómez, J. F., Suárez, O., Gómez, Y., Miranda, L. F., Torrelles, J. M., Anglada, G., & Morata, Ó. 2008, *AJ*, 135, 2074
- Gómez, Y., Tafoya, D., Anglada, G., Miranda, L. F., Torrelles, J. M., Patel, N. A., & Hernández, R. F. 2009, *ApJ*, 695, 930
- Helfand, D. J., Becker, R. H., White, R. L., Fallon, A., & Tuttle, S. 2006, *AJ*, 131, 2525
- Imai, H. 2007, in *Astrophysical Masers and their Environments*, IAU Symp. 242, 279
- Ivison, R. J., Seaquist, E. R., & Hall, P. J. 1994, *MNRAS*, 269, 218
- Jacoby, G. H., & Van de Steene, G. 2004, *A&A*, 419, 563
- Jewell, P. R., Schenewerk, M. S., & Snyder, L. E. 1985, *ApJ*, 295, 183
- Kafatos, M., Hollis, J. M., Yusef-Zadeh, F., Michalitsianos, A. G., & Elitzur, M. 1989, *ApJ*, 346, 991
- Kwok, S. 1993, *ARA&A*, 31, 63
- Kwok, S., Purton, C. R., & Keenan, D. W. 1981, *ApJ*, 250, 232
- Lagadec, E., Verhoelst, T., Mékarnia, D., et al. 2011, *MNRAS*, 412, 1426
- Lewis, B. M. 1989, *ApJ*, 338, 234
- Luo, S. G., Condon, J. J., & Yin, Q. F. 2005, *ApJS*, 159, 282
- Manteiga, M., García-Hernández, D. A., Ulla, A., Manchado, A., & García-Lario, P. 2011, *AJ*, 141, 80
- Meaburn, J., López, J. A., Steffen, W., Graham, M. F., & Holloway, A. J. 2005, *AJ*, 130, 2303
- Miranda, L. F., Fernández, M., Alcalá, J. M., Guerrero, M. A., Anglada, G., Gómez, Y., Torrelles, J. M., & Aaquist, O. B. 2000, *MNRAS*, 311, 748
- Miranda, L. F., Gómez, Y., Anglada, G., & Torrelles, J. M. 2001, *Nature*, 414, 284
- Miranda, L. F., & Solf, J. 1991, *A&A*, 252, 331
- Miranda, L. F., Suárez, O., & Gómez, J. F. 2010, *Lecture Notes and Essays in Astrophysics*, 4, 89
- Norris, R. P., Hopkins, A. M., Afonso, J., et al. 2011, *PASA*, 28, 215
- Paresce, F., & Hack, W. 1994, *A&A*, 287, 154
- Payne, H. E., Phillips, J. A., & Terzian, Y. 1988, *ApJ*, 326, 368
- Pérez-Sánchez, A. F., Vlemmings, W. H. T., & Chapman, J. M. 2011, *MNRAS*, 418, 1402
- Phillips, J. P., & Ramos-Larios, G. 2008, *MNRAS*, 383, 1029
- Pottasch, S. R., & Bernard-Salas, J. 2010, *A&A*, 517, A95
- Pottasch, S. R., Bignell, C., & Zijlstra, A. 1987, *A&A*, 177, L49
- Pottasch, S. R., Olling, R., Bignell, C., & Zijlstra, A. A. 1988, *A&A*, 205, 248
- Purton, C. R., Feldman, P. A., Marsh, K. A., Allen, D. A., & Wright, A. E. 1982, *MNRAS*, 198, 321
- Ramos-Larios et al. 2012, *A&A*, in press
- Ratag, M. A., Pottasch, S. R., Zijlstra, A. A., & Menzies, J. 1990, *A&A*, 233, 181
- Ratag, M. A., & Pottasch, S. R. 1991, *A&AS*, 91, 481
- Reid, M. J., & Moran, J. M. 1981, *ARA&A*, 19, 231
- Reid, M. J., Muhleman, D. O., Moran, J. M., Johnston, K. J., & Schwartz, P. R. 1977, *ApJ*, 214, 60
- Reid, M. J., Schneps, M. H., Moran, J. M., et al. 1988, *ApJ*, 330, 809
- Rodríguez, L. F., et al. 1985, *MNRAS*, 215, 353
- Sahai, R., Morris, M., Sánchez-Contreras, C., & Claussen, M. 2007, *AJ*, 134, 2200
- Sahai, R., Morris, M. R., & Villar, G. G. 2011, *AJ*, 141, 134
- Schneider, S. E., Terzian, Y., Purgathofer, A., & Perinotto, M. 1983, *ApJS*, 52, 399
- Seaquist, E. R., & Davis, L. E. 1983, *ApJ*, 274, 659
- Seaquist, E. R. 1991, *AJ*, 101, 2141
- Sevenster, M. N. 2002, *AJ*, 123, 2772
- Sevenster, M. N., Chapman, J. M., Habing, H. J., Killeen, N. E. B., & Lindqvist, M. 1997a, *A&AS*, 122, 79
- Sevenster, M. N., Chapman, J. M., Habing, H. J., Killeen, N. E. B., & Lindqvist, M. 1997b, *A&AS*, 124, 509
- Sevenster, M. N., van Langevelde, H. J., Moody, R. A., Chapman, J. M., Habing, H. J., & Killeen, N. E. B. 2001, *A&A*, 366, 481
- Shepherd, M. C., Cohen, R. J., Gaylard, M. J., & West, M. E. 1990, *Nature*, 344, 522
- Sopka, R. J., Herbig, G., Kafatos, M., & Michalitsianos, A. G. 1982, *ApJ*, 258, L35
- Suárez, O. 2004, Ph.D. Thesis, Universidad de Vigo, Spain
- Suárez, O., Gómez, J. F., Miranda, L. F., et al. 2009, *A&A*, 505, 217
- Suárez, O., Gómez, J. F., & Morata, O. 2007, *A&A*, 467, 1085
- Tafoya, D., Gómez, Y., Anglada, G., et al. 2007, *AJ*, 133, 364
- Tafoya, D., Gómez, Y., Patel, N. A., et al. 2009, *ApJ*, 691, 611
- Uscanga, L., Gómez, Y., Raga, A. C., et al. 2008, *MNRAS*, 390, 1127
- Van de Steene, G. C., & Jacoby, G. H. 2001, *A&A*, 373, 536
- Van de Steene, G. C. M., & Pottasch, S. R. 1993, *A&A*, 274, 895
- Van de Steene, G. C., & Pottasch, S. R. 1995, *A&A*, 299, 238
- van der Veen, W. E. C. J., & Habing, H. J. 1988, *A&A*, 194, 125
- Velázquez, P. F., Gómez, Y., Esquivel, A., & Raga, A. C. 2007, *MNRAS*, 382, 1965
- White, R. L., Becker, R. H., & Helfand, D. J. 2005, *AJ*, 130, 586
- Zhang, C. Y., & Kwok, S. 1991, *A&A*, 250, 179
- Zijlstra, A. A., te Lintel Hekkert, P., Pottasch, S. R., et al. 1989, *A&A*, 217, 157
- Zuckerman, B., & Lo, K. Y. 1987, *A&A*, 173, 263

Table 1. VLA archival data used

Project ID	Config ^a	Frequency MHz	Type ^b	Observing Date
SEAQ	A	1465	cont	1982-FEB-82
	A	4885	cont	1982-FEB-82
AP076	C	4860	cont	1984-APR-23
	C	4860	cont	1984-APR-24
AP116	B	4860	cont	1986-JUL-26
AP121	BC	14940	cont	1986-SEP-17
AP125	C	4860	cont	1986-NOV-14
	C	4860	cont	1986-DEC-11
AP128	C	4860	cont	1987-JAN-17
AS280	A	22460	cont	1987-JUL-21
AP166	A	8440	cont	1988-NOV-06
VFB01	BC	1615	cont	1990-OCT-18
SEAQ	A	1612	OH	1982-FEB-82
AH100	BC	1612	OH	1985-JUN-23
AP163	D	1612	OH	1988-AUG-08
AH185	A	1612	OH	1988-OCT-30
AZ030	D	1612	OH	1987-MAR-25
AP128	C	1665	OH	1987-JAN-17

^(a) Configuration of the VLA ^(b) Type of observation: cont (continuum), OH (OH maser)

Table 2. Confirmed OHPNe

Object ID	IRAS	PN G ^a	Common name	Continuum position		Error ^b (")	OH position		Error ^b (")	Position difference (")	References ^c	Notes
				RA (J2000)	Dec (J2000)		RA (J2000)	Dec (J2000)				
1	17103–3702	349.5+01.0	NGC 6302	17 13 44.5	–37 06 11	3	17 13 44.40	–37 06 09.6	3	2	6	^d
2	17347–3139			17 38 00.61	–31 40 55.0	0.8	17 38 00.57	–31 40 54.9	0.8	0.5	4	^d
3			JaSt 23	17 40 23.08	–27 49 12.3	0.4	17 40 23.07	–27 49 11.4	2.4	0.9	2,3,6	^e
4	17393–2727			17 42 33.14	–27 28 24.7	0.8	17 42 33.16	–27 28 24.6	2.4	0.3	1, 2, 6	
5	19219+0947	045.4–02.7	Vy 2–2	19 24 22.218	+09 53 56.33	0.09	19 24 22.207	+09 53 56.14	0.22	0.25	6	
6	19255+2123	056.0+02.0	K 3–35	19 27 44.026	+21 30 03.57	0.20	19 27 44.022	+21 30 03.31	0.20	0.2	5	^d

References. (1) Zijlstra et al. (1989); (2) Sevenster et al. (1997a); (3) Van de Steene & Jacoby (2001); (4) Tafuya et al. (2009); (5) Gómez et al. (2009); (6) this paper

^(a) Designation of galactic planetary nebulae in the catalog of Acker et al. (1992) ^(b) The position uncertainty estimated for radio interferometric observations is of the order of 1/10 of the synthesized beam, to be conservative we considered a positional error of $\sim 1/5$ of the synthesized beam (See Sect. 2.3). ^(c) Literature reference for the quoted positions. ^(d) Simultaneous OH and continuum observations ^(e) The relationship of JaSt 23 with IRAS 17371–2747 is uncertain.

Table 3. Possible OHPNe

IRAS	PN G	Continuum position		Error (")	OH position		Error (")	Position difference (")	References
		RA (J2000)	Dec (J2000)		RA (J2000)	Dec (J2000)			
17150–3754		17 18 28.97	–37 58 01.9	0.4	17 18 28.922	–37 58 01.79	2.0	0.6	3
17168–3736		17 20 15.08	–37 39 31.5	1.1	17 20 15.047	–37 39 34.31	2.4	2.8	2,3
17221–3038	356.1+02.7	17 25 19.37	–30 40 42.3	0.6	^a				3
17375–2759		17 40 38.57	–28 01 00.4	0.7	17 40 38.587	–28 01 01.08	2.4	0.7	1, 2

References. (1) Pottasch et al. (1988); (2) Sevenster et al. (1997a); (3) this paper

^(a) No interferometric OH observation available

Table 4. Misclassified OHPNe

IRAS	OH position		References	Notes
	RA (J2000)	Dec (J2000)		
17207–2856				^a
17375–3000	17 40 43.339	–30 02 04.86	1	
17418–2713	17 44 58.723	–27 14 43.37	1	^b
17443–2949	17 47 35.442	–29 50 53.32	2	^b
17580–3111	18 01 20.399	–31 11 20.55	2	^c

References. (1) Sevenster et al. (1997a); (2) Gómez et al. (2008)

^(a) Neither radio continuum nor OH emission was detected ^(b) Possible AGB star ^(c) Possible post-AGB star